Optimal (Dynamic) Turbine Repositioning Strategies for a Floating Wind Farm Depending on Mooring Line Stiffness

Starink, Leendert; Xie, Zhaochen; Becker, Marcus; Van Den Berg, Daniel; Van Wingerden, Jan Willem

DOI
10.1088/1742-6596/3131/1/012039

Publication date
2025

Document Version
Final published version

Published in
Journal of Physics: Conference Series

Journal of Physics:
Conference Series

PAPER • **OPEN ACCESS**

Optimal (Dynamic) Turbine Repositioning Strategies for a Floating Wind Farm Depending on Mooring Line Stiffness

To cite this article: Leendert Starink *et al* 2025 *J. Phys.: Conf. Ser.* **3131** 012039

Journal of Physics: Conference Series **3131** (2025) 012039 doi:10.1088/1742-6596/3131/1/012039

Optimal (Dynamic) Turbine Repositioning Strategies for a Floating Wind Farm Depending on Mooring Line Stiffness

Leendert Starink[1], Zhaochen Xie[1], Marcus Becker[1], Daniel van den Berg[1], Jan-Willem van Wingerden[1]

[1]Delft Center for Systems and Control, TU Delft, Delft, The Netherlands.

E-mail: l.starink@tudelft.nl

Abstract. In the pursuit of mitigating the wake effect, floating wind turbines have additional degrees of freedom compared to their fixed-bottom counterparts. The mooring system with which floating wind turbines are anchored to the seabed allows a range of motion in which turbines can be repositioned. Turbine repositioning uses yaw control to reposition floating wind turbines, and to thereby actively optimize the wind farm layout. Previous research has focused on obtaining optimal steady-state yaw angles for turbine repositioning by using steady-state wake models. Here, the primary conclusion is that mooring line tension needs to be relaxed to facilitate a range of movement large enough for steady-state turbine repositioning to be effective. The presented work studies the effect of using dynamic yaw signals for turbine repositioning by using a dynamic wake model. To study the effect of including wake dynamics, an optimization problem to find the optimal yaw control signals for a two turbine floating wind farm is solved for various mooring configurations. This work shows that for stiffer mooring configurations, turbine repositioning can still be leveraged to increase wind farm efficiency, but that the optimal yaw control action is dynamic for these cases.

1 Introduction

Offshore wind energy has become a cornerstone in the transition to renewable energy sources. With a current installed capacity of 35 GW in Europe, and a planned installed capacities of 60 GW and 300 GW in 2030 and 2050, wind energy is scheduled to grow exponentially in the coming decades [13]. Installation sites that are favorable for wind energy, meaning that they have high average wind speed and shallow water depth, to facilitate this growth are however not abundantly available. The benefit of floating wind farms (FWFs) is that they expand the attainable wind energy resources immensely by enabling farms to be installed in deeper waters, where conventional bottom fixed installation is economically unattractive.

Within a wind farm, wind turbines experience reduced wind speeds when the wind direction aligns with the location of upstream turbines in the farm. Because, as an upstream turbine extracts energy from the wind, it leaves behind an area of low wind speed, which a downstream turbine experiences. This is known as the wake effect. Wind farm control methods that mitigate the wake effect, e.g. wake steering, have mainly been studied for bottom-fixed wind turbines. Floating wind turbines (FWTs) offer additional degrees of freedom, as each turbine can move within the constraints of its mooring lines. This mobility can be leveraged for wake steering, allowing turbines to be repositioned in the crosswind direction to prevent the wake from overlapping with downwind counterparts. By adjusting the turbine's yaw angle,

a misalignment with the incoming wind is created, resulting in an aerodynamic force component in the crosswind direction, which facilitates the repositioning [5, 6].

Preliminary results on turbine repositioning indicate promising increases in wind farm efficiency [8, 9]. However, they also highlight the need to significantly reduce mooring line tension to enable a range of movement sufficient for the effective implementation of this technique. Furthermore, it has become clear that wake steering for FWFs is different to the fixed-bottom case in two key ways. First, the downstream turbines can also benefit from yaw misalignment, as it can move itself out of the wake of an upstream turbine. Second, yaw misalignment steers the wake in one direction, but repositions the turbine in the opposite direction. Because these mechanisms counteract each other, this can negate the wake steering effect [11]. The effect of floating turbine repositioning is currently mainly assessed using steady-state wake models. In this way wake dynamics are not modeled, and it is only possible to optimize the yaw angles such that they yield the optimal turbine repositioning in steady-state. Preliminary work on turbine repositioning with a dynamic wake model is done, but only considers the case where mooring lines are significantly lengthened [10]. To better understand wake steering for floating wind turbines, the motivation for this work is to analyze turbine repositioning with dynamic models, while also considering the stiffness of the mooring configuration.

Therefore, this work contributes in two key ways; namely 1) by evaluating the effect of including wake dynamics in the assessment of turbine repositioning, and 2) by assessing the effect of the stiffness of the mooring configuration on turbine repositioning when wake dynamics are included. In this paper it is investigated how the mooring configuration influences the floater dynamics, and how these dynamics influence the optimal turbine repositioning solution. The presented work uses the dynamic wake model FLORIDyn [3] to include wake dynamics and thereby find optimal time-varying yaw signals. An FWT model with a semi-submersible platform is coupled with FLORIDyn to identify optimal yaw actions over time for a two-turbine FWF across a finite time horizon.

The remainder of this paper is structured as follows: first the simulation environment is introduced in Section 2 by introducing the floating turbine model and FLORIDyn. The optimization problem is defined in Section 3, and finally, the results are analyzed and presented in Section 4.

2 Description of the simulation framework

To define a simulation environment, this section first covers a simplified floater model based on the work of Homer and Nagamune [7]. This floater model captures the surge and sway dynamics of the turbines, and is coupled to FLORIDyn, which models wakes and the dynamic interaction between wakes. Next, FLORIDyn and the coupling between the floater model and FLORIDyn are covered. This section is concluded by covering the details regarding the wind farm layout and simulation settings used for the results in the remainder of this work.

2.1 Modeling of the floater dynamics

A simple floater model is derived by considering all forces that act on the platform, and by using these forces to construct the differential equation that governs the dynamics

$$m\ddot{p} = F_{\text{aero}}\left(\dot{p}, v(p), \gamma\right) + F_{\text{hydro}}(\dot{p}) + F_{\text{mooring}}(p), \tag{1}$$

where p is the position vector of the turbine consisting of the displacement in sway and surge direction. The time derivative of p is denoted by $\dot{p}$, and all forces on the right hand side of the equation are nonlinear functions that depend on p, $\dot{p}$, the turbine's yaw angle γ, and the effective wind speed at the turbine location $v(p)$. The mass m represents the combined mass of the turbine, the floater, and added mass resulting from Morison's equation on which will be commented in Section 2.1.2. Each of the forces will now be defined in more detail.

2.1.1 The aerodynamic thrust force models the thrust force that acts on the rotor, and is a function of the turbine's yaw angle, the effective wind speed at the location of the turbine, and the turbine's velocity. The modeling of the aerodynamic thrust force follows the vortex cylinder model of a yawed actuator disc [4], and is defined as:

$$F_{\text{aero}}\left(\dot{p}, v(p), \gamma\right) = \frac{1}{8}\pi\rho_{\text{a}}D^2 C_{\text{T}}(\dot{p}, v(p), \gamma)\|\dot{p} - v\|_2^2 \begin{bmatrix}\cos(\gamma)\\ \sin(\gamma)\end{bmatrix}, \tag{2}$$

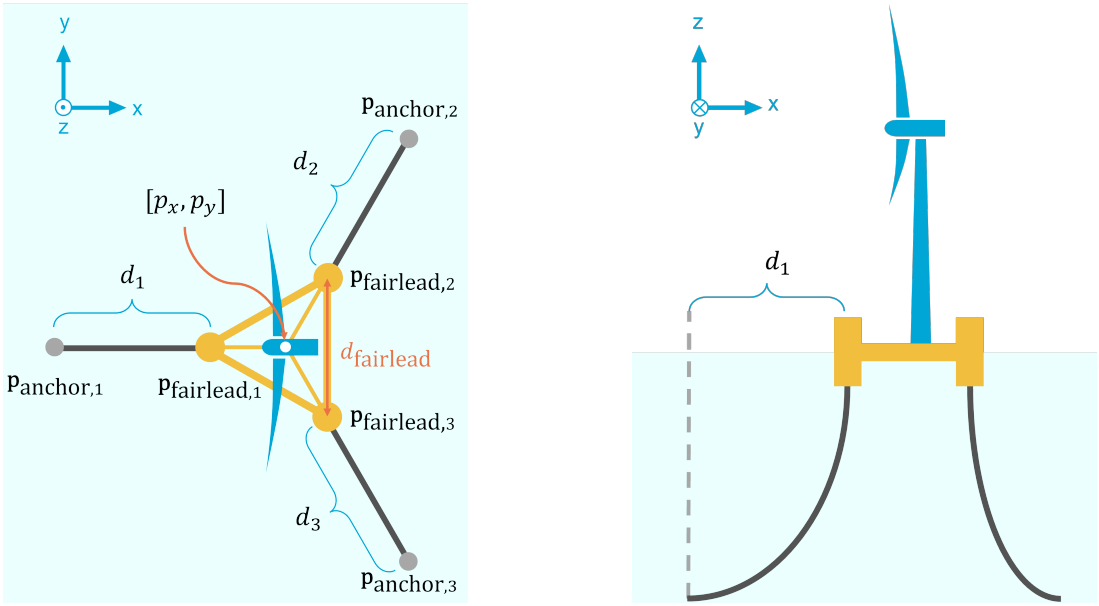

(a) top view (X-Y plane) (b) side view (X-Z plane)

Figure 1: Illustration of the location of the anchors, fairleads, and mooring lines. The position of the turbine p is indicated at the center of the platform.

where D is the rotor diameter, ρ_a is the air density, and C_T is the thrust coefficient that is modeled as

$$C_T(\dot{p}, v(p), \gamma) = 4a\left(\cos\gamma_{rel} + \tan\frac{p}{2}\sin\gamma_{rel} - a\sec^2\frac{X}{2}\right). \tag{3}$$

Here, a is the axial induction factor which is fixed to $1/3$, $\gamma_{rel} = \gamma - \arctan\frac{v_x - \dot{p}_x}{v_y - \dot{p}_y}$ is the relative yaw angle, and $X = (0.6a + 1)\gamma_{rel}$ is the wake skew angle immediately past the rotor. The thrust coefficient is modeled while taking into account the relative wind speed, and the relative yaw angle experienced by the turbine caused by the velocity of the turbine itself.

2.1.2 The hydrodynamic forces that act on the platform are modeled using Morison's equation. The simulations in this work are performed under the condition of no current in the water. Hence, all hydrodynamic drag results from the velocity of the turbine itself. The hydrodynamic drag force is modeled as

$$F_{hydro}(\dot{p}, \ddot{p}) = \underbrace{\frac{1}{2}\rho C_d A_d \dot{p}\|\dot{p}\|_2}_{\text{Drag force}} - \underbrace{\rho_w C_m A_m \ddot{p}}_{\text{Mass force}}, \tag{4}$$

with ρ_w the density of water, and the coefficients C_d, A_d denoting the drag coefficient and reference area for the drag term, and C_m, A_m denoting the drag coefficient and reference area for the mass term. The hydrodynamic force can be split into a drag term that is related to the velocity of the floater, and a hydrodynamic mass term proportional to the floater acceleration. As mentioned earlier, the mass term is incorporated into the total mass at the left hand side of Equation 1, since it is proportional to the acceleration of the turbine.

2.1.3 The mooring force that acts on the floater is modeled with use of the OC4 design for a semisubmersible platform by NREL [12]. This design has three mooring lines oriented at 120° angles with respect to each other, and is schematically visualized in Figure 1. The mooring line anchors lie 200 meters below sea level, and by default, at a radial distance of 837.6 meters from the platform centerline in the horizontal plane. To adapt the stiffness of the mooring system this radial distance will be varied in the optimization. Shortening this radial distance while keeping the mooring line length constant results in slacker mooring

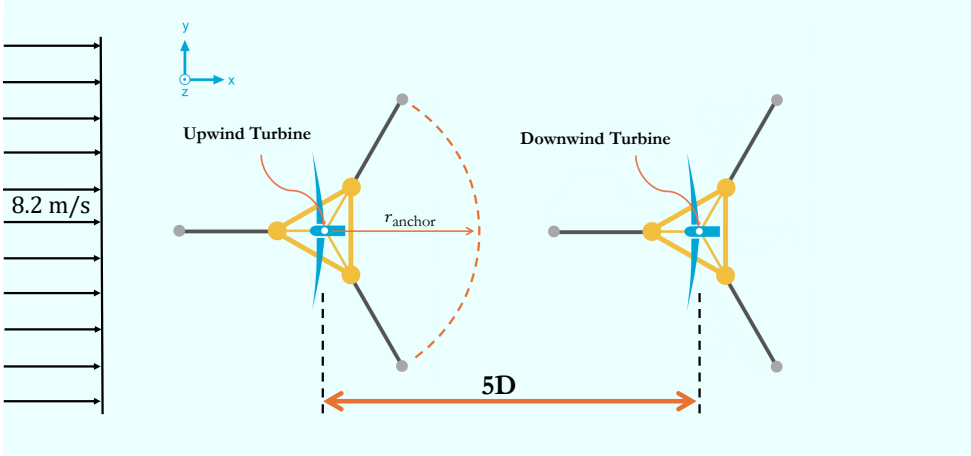

Figure 2: Wind farm layout and mooring configuration. The anchoring radius which is varied in the optimization is indicated, and is equal to the distance from the platform center line to the anchor. Note that this a schematic representation, and that the proportions in this image are intentionally distorted.

lines, and hence a reduced stiffness of the mooring configuration. The total mooring force that acts on the platform equals the combined forces of the separate mooring lines:

$$F_{\text{mooring}}(p) = \sum_{i=1}^{3} F_{\text{mooring},i}(p_{\text{anchor},i} - p_{\text{fairlead},i}(p)), \tag{5}$$

where the mooring force for each mooring line depends on the horizontal distance between the anchor and the fairlead of that mooring line. The force is evaluated based on interpolation from a lookup table provided along with the definition of the semi-submersible platform [12].

2.2 Wake modeling

FLORIDyn [1] is a dynamic parametric engineering model used to simulate the wake interaction between turbines at a low computational cost. To this end the model employs so-called Observation Points (OP), which are created at each time step at each rotor center. Since the turbines move in this work, also the OP creation location changes, respectively. The OPs inherit the turbine state (e.g., yaw angle and turbine induction) at the time of their creation and travel with the free wind speed and direction downstream. Turbines located in the wake of other turbines use the passing OPs and their states to estimate the wind speed deficit resulting from the wake. The employed version of FLORIDyn[1] [2] uses the Gauss-Curl-Hybrid model to model the wind speed reduction. Note that no wake modifications have been made to the model to account for a possibly different wake recovery due to the turbine movement. This is justifiable for this preliminary study as the turbine speeds observed with the results are fairly slow. However, future work should further investigate this assumption.

2.3 Wind farm model

To complete the simulation environment, FLORIDyn is coupled to the floater model. To couple the models, FLORIDyn receives the location of the tower bases at every simulation time step from the floater model. Based on the position of the bases, FLORIDyn computes the effective wind speeds at these locations, and creates a new OP for each turbine originating from the location of its base. In turn, the floater model receives the effective wind speed from FLORIDyn and uses this to compute the aerodynamic force on the rotor for this time step. To compute the power at a given time step, the effective wind speed from FLORIDyn, and the velocity of the floater are used to compute the effective wind speed experienced by the turbine.

For all simulations performed in this work, an FWF consisting of two 5 MW turbines mounted on semi-submersible platforms is used. The turbines are spaced five rotor diameters apart, and the layout

[1] Code available at https://github.com/TUDelft-DataDrivenControl/OFF

is schematically illustrated in Figure 2. The wind conditions are constant in time, and are equal in all simulations. The wind is assumed to be constant at 8.2 meters per second, and the wind direction is aligned with the positive x-axis. The distance r_{anchor}, indicated in Figure 2 serves as a measure to adapt the stiffness of the mooring system. In the original design, this distance is equal to 837.6 meters, and this distance can be decreased to slacken the mooring lines. Thereby the stiffness of the system can be changed. For all simulations in this work the turbines are initialized from an equilibrium position. Meaning that, prior to the simulation being started, the turbine positions are calculated for which the aerodynamic force on the rotor is in equilibrium with the mooring forces.

3 Description of the optimization problem

We will formulate an optimization problem with the goal to find the yaw signals that maximize the energy production of the wind farm over a period of 1800 seconds. To achieve this, the yaw signals are discretely sampled at a 25 second interval, and are provided to the optimizer as decision variables. For the two turbine wind farm the decision variables are therefore

$$\Gamma = \begin{bmatrix} \gamma_{1,0} & \gamma_{1,25} & \cdots & \gamma_{1,1800} \\ \gamma_{2,0} & \gamma_{2,25} & \cdots & \gamma_{2,1800} \end{bmatrix} \in \mathbb{R}^{2\times 73}, \tag{6}$$

resulting in 73 decision variables per turbine. During the simulation, the yaw angles are linearly interpolated between the setpoints. Next, the cost function is defined as

$$J(\Gamma, r_{\text{anchor}}) = \frac{1}{T}\sum_{i=1}^{N}\sum_{j=1}^{T} P_{i,j}, \tag{7}$$

where $P_{i,j}$ is the power produced by the i'th turbine at the j'th simulation time step. The cost is normalized by the total number of time steps T, and is therefore equal to the average power production of the wind farm. It is also indicated that the cost function depends on r_{anchor}, which determines the mooring configuration. The optimal yaw signals are defined with the following maximization criterion

$$\Gamma^*_{r_{\text{anchor}}} = \underset{\Gamma}{\text{argmax}}\, J, \tag{8}$$

where it is indicated that a set of yaw signals is only optimal with respect to a certain mooring configuration. To assess the effect of the anchoring radius on the optimal solution, the maximization criterion will be evaluated for different anchoring radii. Lastly, to formulate the full optimization problem, a yaw rate constraint is added to guarantee continuity of the yaw signals, and a constraint on the maximum yaw excursion is added to guarantee validity of the vortex cylinder model of a yawed actuator disc. This results in:

$$\begin{aligned} &\max_{\Gamma} J \\ &\text{s.t} \quad \begin{cases} \gamma_{i,0} = 0 & \forall i & \text{Initial condition} \\ |\gamma_{i,j}| \le \phi & \forall i,j & \text{Constraint on the maximum yaw angle} \\ |\gamma_{i,j+1} - \gamma_{i,j}| \le \theta & \forall i,j & \text{Constraint on the yaw rate} \end{cases} \end{aligned} \tag{9}$$

where the maximum yaw angle is fixed to ϕ, and the maximum yaw rate is fixed to 0.3 degrees per second. For the maximum yaw angle, two cases are studied. One case where $\phi = 45$ degrees, and a more restrictive case with $\phi = 20$ degrees. Also, a constraint is added to ensure that all simulations start from the same initial condition. To compare the results from this optimization problem to steady-state repositioning, we formulate a second optimization problem to find the optimal steady-state solutions:

$$\begin{aligned} &\max_{\Gamma} J \\ &\text{s.t} \quad \begin{cases} |\gamma_{i,j}| \le \phi & \forall i,j & \text{Constraint on the maximum yaw angle} \\ |\gamma_{i,j+1} - \gamma_{i,j}| = 0 & \forall i,j & \text{Constant yaw signals in time} \end{cases} \end{aligned} \tag{10}$$

where to obtain the steady-state optimum, we assert that the yaw signals are constant in time. Also, the initial condition constraint is lifted.

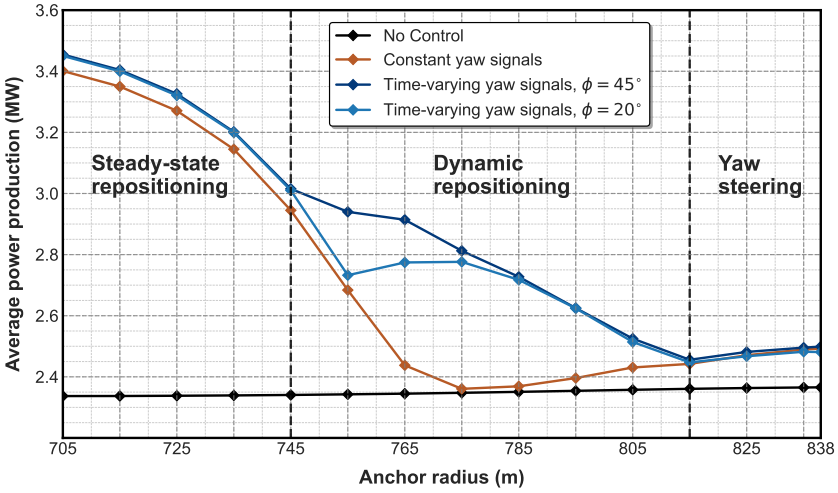

Figure 3: The optimized wind farm power outputs compared to the no control case. The optimization result where the optimizer has all degrees of freedom is shown in dark blue for $\phi = 45$ degrees, and in light blue for $\phi = 20$ degrees. The optimization result where constant yaw angles are enforced is shown in orange. It is visible that for anchoring radii in the range of 745 to 815 meters the optimal solutions with full freedom significantly outperform the steady-state optima. Thus, for these cases it shows that it is suboptimal to apply steady-state techniques. Three regions are indicated, in each of which a different wake steering technique is optimal.

4 Results

The optimization problem is solved for different locations of the mooring line anchors. To analyze the effect of mooring stiffness on the optimal repositioning solution, the optimization problem is solved for anchor radii in the range of 705 to 837.6 meters. Here, the stiffest configuration conforms to the OC4 mooring design. Also, to study the effect of limiting the maximum yaw angle, the optimization problem is solved for $\phi = 45$ and 20 degrees. The results of the optimization are presented in Figure 3. Here, the optimized wind farm power output is compared to the no control case, and compared to the power production with the optimal constant angles. In the figure, there are three regions indicated that refer to three optimal repositioning techniques, which will be discussed later.

It is most interesting to compare the constant yaw optima to the optimal solutions where time-varying yaw signals are allowed. For the slackest configurations, and for the tautest configurations, the optima with full yawing freedom are close to the constant yaw optima. However, for anchoring radii in the range of 750 to 810 meters, the optimal results where time-varying yawing is allowed drastically outperform the constant yaw optima.

We will show that there are in fact three wake steering techniques at play. In the first case, for the slackest configurations, it is optimal to perform steady-state turbine repositioning. Second, for the intermediate cases, it is optimal to dynamically yaw the turbines to achieve dynamic turbine repositioning. Third, for the most taut cases, it is again optimal to apply steady-state yaw signals. However, not with the goal of repositioning the turbines, but to perform conventional yaw steering which has been proposed for fixed-bottom wind farms. Each of the techniques is now treated in greater detail by looking at the optimal yaw control signals, and the optimal turbine trajectories.

4.1 Steady-state repositioning

The cases where steady-state turbine repositioning is optimal are shown in Figure 4. In this figure, the optimized yaw signals for $\phi = 45$ degrees, together with the crosswind turbine trajectories for an anchoring radius of 705 up to 745 meters are shown. From the figure, notice that the signals are close to a steady-state value for the majority of the optimization horizon. For steady-state turbine repositioning, the main wake steering mechanism is repositioning the turbines. Notice that the control of both turbines is equally important. This is because wake deflection caused by yaw misalignment is counterproductive to the repositioning effect. Therefore, to achieve a crosswind distance between the turbines that is sufficient for the method to be effective, both turbines need to be repositioned. As the anchoring radius increases,

the stiffness of the mooring system also increases. Therefore, from Figure 4 it is visible that more yawing effort is required to achieve a similar crosswind repositioning as the anchoring radius increases.

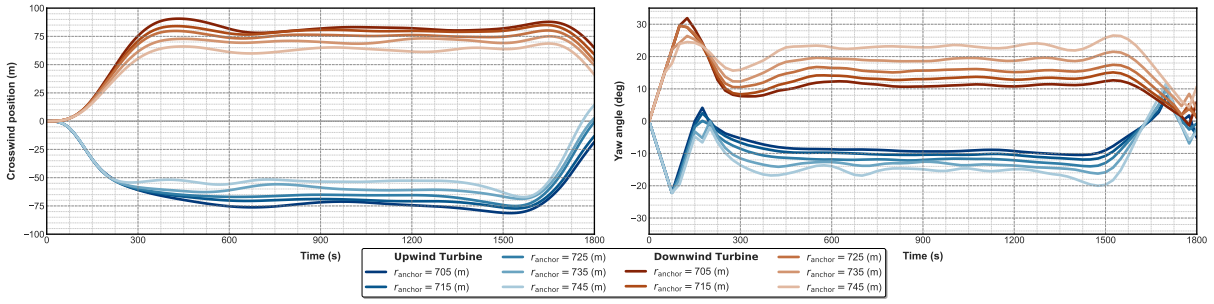

Figure 4: Optimal crosswind trajectories and optimal yaw signals for the mooring configurations with anchoring radius 705 to 745 meters, and $\phi = 45$ degrees. The optimal trajectories show a steady-state repositioning technique, where the upwind turbine is repositioned in the negative crosswind direction, and the downwind turbine is repositioned in the positive crosswind direction. Note that the optimal yaw signals are in steady-state apart form the beginning and the end of the optimization horizon.

4.2 Dynamic repositioning

By including wake dynamics in the analysis of turbine repositioning for stiffer mooring configurations, this work presents a novel floating turbine repositioning technique: dynamic repositioning. To illustrate dynamic repositioning, Figure 5 presents the optimal yaw signals and optimal crosswind trajectories for anchoring radii of 755, 785 and 805 meters, for the case $\phi = 45$ degrees. For the reason of conciseness, three of the six cases where dynamic repositioning is optimal are shown. For dynamic repositioning, notice that the optimal yaw solutions are periodic in nature, and lead to sinusoidal crosswind trajectories. By comparing the trajectories of the case with an anchoring radius of 755 meters in Figure 5a, to the cases with anchoring radius 785, and 805 meters, in Figures 5b and 5c respectively, it becomes visible that the optimal yawing frequency becomes larger as the mooring stiffness increases.

Further analysis shows that the optimal yawing frequency is related to the natural frequency of the mooring system. In essence, the floater dynamics are those of a large nonlinear mass-spring-damper system. By linearizing the floater dynamics around their equilibrium positions with $\gamma = 0$, in Figure 6a, a Bode magnitude plot is made of the transfer function from the yaw angle to the crosswind position for each of the mooring configurations where dynamic repositioning is optimal. Notice that as the anchoring radius increases, the spring stiffness of the system increases, and thereby also the natural frequency of the system increases. It is important to mention that the nonlinear model has higher damping than the linearization, resulting in the gain at the natural frequency to be smaller for the nonlinear case.

Accompanying the figure is a table indicating how the natural frequencies relate to optimal yawing frequencies. To make this comparison, the natural frequency of the platform in crosswind direction, indicated by ω_0, is compared to the frequency at which the yaw signal of the upwind turbine contains the most power, indicated by $\omega_{\gamma 1}$. This frequency is obtained by computing the power spectrum of the yaw signal, and taking the frequency that contains the most power. Notice that, while there is not a direct linear correlation, the optimal yawing frequency and the platform natural frequency are related.

Dynamic repositioning is capable of improving the wind farm efficiency by exploiting two features of the dynamics. Firstly, the optimal yaw signals are periodic close to the natural frequency of the mooring system. By yawing close to this frequency, the magnitude of the crosswind trajectories is maximized. Secondly, the phase shift between the yaw signals alleviates the negative coupling between wake deflection from yaw misalignment, and wake deflection from repositioning. As the wake of the upwind turbine requires time to travel downstream, the effects of it are experienced by the second turbine with a time delay. The phase shift between the turbine trajectories is optimized such that the overlap of the upwind wake with downwind rotor is minimized over time.

Finally, notice from Figure 3, that for the case with a yaw limit of $\phi = 20$ degrees, the steady-state repositioning technique is optimal for the anchoring radius of 755 meters. Furthermore, for the anchoring radii of 765 and 775 meters, the gain in average power is less due to the yawing constraint. Hence, it can be seen that limiting the yaw action also limits the range where dynamic repositioning is effective.

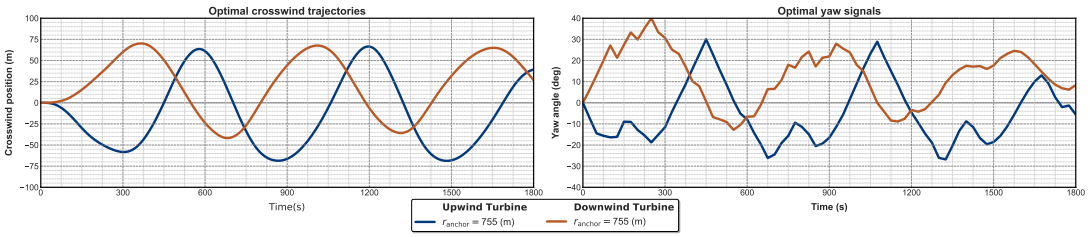

(a) Optimal solution for $r_{\text{anchor}} = 755$ meters

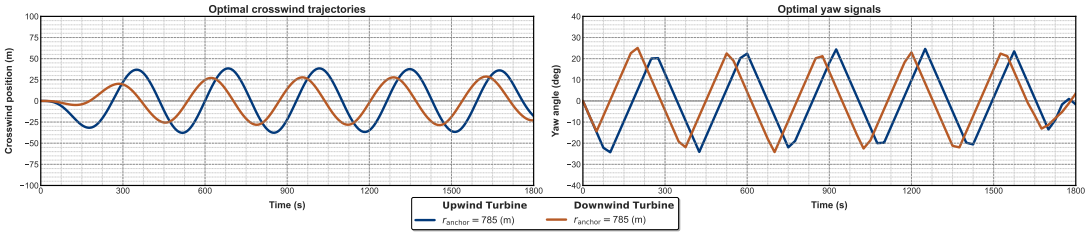

(b) Optimal solution for $r_{\text{anchor}} = 785$ meters

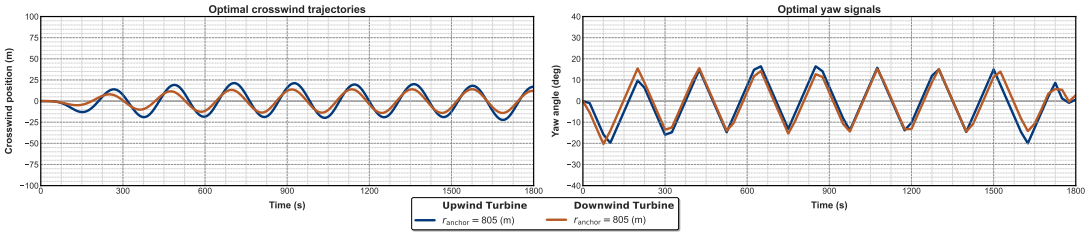

(c) Optimal solution for $r_{\text{anchor}} = 805$ meters

Figure 5: Optimal crosswind trajectories for anchoring radii 755, 785, and 805 meters and $\phi = 45$ degrees, showing a dynamic repositioning technique. Here the crosswind trajectories are sinusoidal, and the optimal yaw signals are periodic. Notice that for an increasing anchoring radius, and therefore an increasing mooring stiffness, the optimal yawing frequency increases.

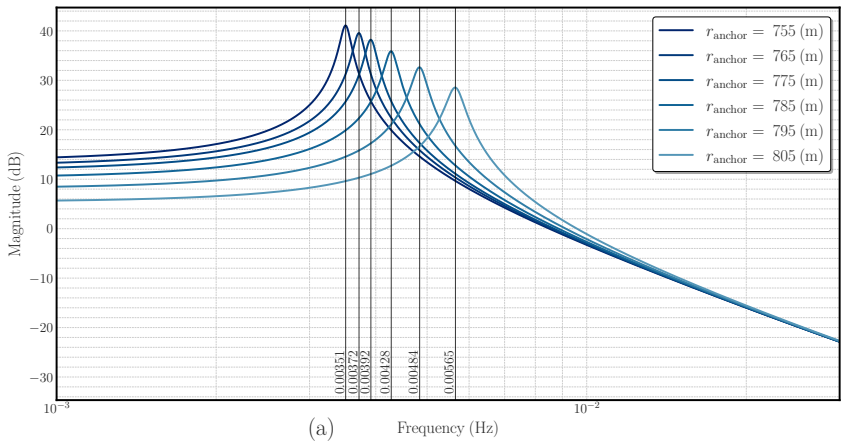

(a)

r_{anchor} (m)	ω_0 (mHz)	ω_{γ_1} (mHz)
755	3.51	1.603
765	3.72	2.105
775	3.916	2.273
785	4.278	2.99
795	4.84	3.66
805	5.654	4.569

(b)

Figure 6: Bode diagram of the linearized dynamics from the yaw angle in degrees, to the crosswind position in meters. The Bode diagram is plotted for the cases where dynamic repositioning is optimal, and the natural frequency of the linearized dynamics is indicated for each case. The table accompanying the plot displays the natural frequencies of the linearized dynamics, and compares them to the frequency that contains the most power in the power spectral density of the optimized yaw angles of the upwind turbine for the case where $\phi = 45$ degrees.

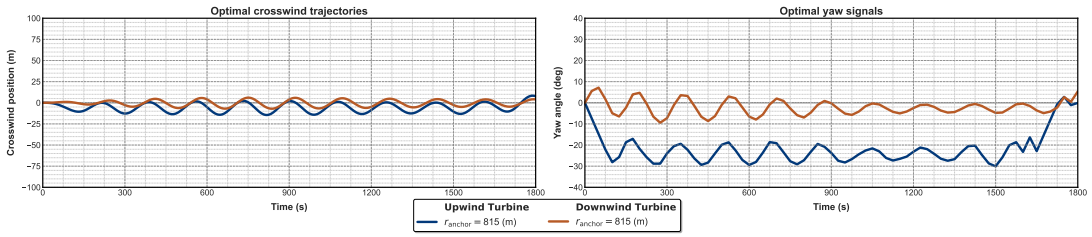

(a) Optimal solution for $r_{\text{anchor}} = 815$ meters

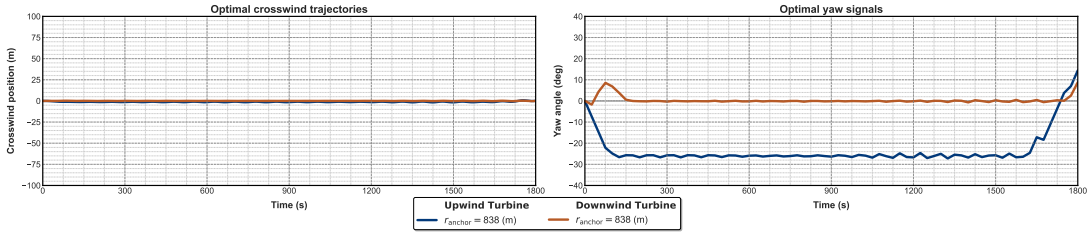

(b) Optimal solution for $r_{\text{anchor}} = 838$ meters

Figure 7: Optimal crosswind trajectories for anchoring radii 815 and 838 meters and $\phi = 45$ degrees, showing a conventional yaw steering technique. While the 815 meter case shows the transition from dynamic repositioning, in the 838 meter case the emphasis has almost completely shifted to yawing of the upwind turbine. Notice that the crosswind repositioning is minimal for these cases.

4.3 Yaw steering

For the most taut mooring configurations the optimizer prefers a technique that resembles conventional yaw steering. To illustrate this, Figure 7 presents the optimal yaw signals and crosswind trajectories for the anchoring radii of 815 and 835 meters. From this figure it is important to notice two things: first, the crosswind repositioning of both turbines is minimal, and second, the emphasis for the yaw control has shifted towards the upstream turbine. In Figure 7a, presenting the case with anchoring radius equal to 815 meters, the optimal yaw signals still contain some periodic yawing, and this case shows the transition of dynamic repositioning to conventional yaw steering. However, as Figure 3 indicates, this offers minimal wind farm efficiency gain over steady-state yawing. By looking at the results for the 837.6 meter case in Figure 7b, the optimal yaw signals are approximately constant. Therefore, for the most taut cases, the optimal wake steering technique is conventional yaw steering, as the wind farm now more resembles a bottom-fixed farm.

5 Conclusion

Analysis with steady-state wake models has shown that mooring line tension needs to be reduced significantly for steady-state turbine repositioning to be effective. By performing an analysis with a dynamic wake model, this work concludes that, for the NREL 5MW turbine with a semi-submersible platform, also for stiffer mooring configurations a gain in wind farm efficiency can be made. For these stiffer mooring configurations it is shown that it is optimal to provide dynamic yaw signals to the turbines, that thereby result in dynamic turbine repositioning. By exploring the optimal yaw signals for various mooring configuration this work concludes that; for slack mooring configurations it is optimal to provide steady-state yaw signals to the turbines, for more taut mooring configurations it is optimal to provide dynamic yaw signals to the turbines, and for the tautest configurations it is optimal to perform traditional yaw steering.

For the dynamic repositioning technique to be feasible, mooring line tension still needs to be reduced comparative to the original OC4 semi-submersible design from NREL. In the original design, the mooring line anchoring radius was set at 837.6 meters. Dynamic repositioning becomes feasible for anchoring radii smaller than 815 meters, and static repositioning becomes optimal for anchoring radii smaller than 755 meters. Because the slackest configurations, where the steady-state repositioning technique is optimal, provide higher wind farm efficiencies than the dynamic repositioning cases, dynamic repositioning provides a midway solution between decreasing mooring stiffness and increasing wind farm efficiency. For dynamic repositioning to be optimal, large yaw angles are required for some mooring configurations. With a more

strict constraint on the maximum yaw angle, the range of mooring configurations where the technique is effective is slightly reduced.

This work has provided the first insights into dynamic repositioning. The objective for future research on this topic should be to validate the results from this work. Since a low-fidelity turbine model is used, it should be investigated if dynamic repositioning is feasible by performing simulations with higher fidelity models. Here, the influence of non-constant wind fields and of waves is also a topic of interest. Lastly, the focus of the optimization in this work has been on maximizing power production. For future work it is interesting to include other factors into the optimization. For example, the effects that these techniques have on mooring line fatigue and the interconnection with the grid.

Acknowledgments
The authors thank S.P. Mulders (TU Delft, DCSC) for his valuable contributions to this work. This work has received support from the FLOATFARM project, funded by the European Union's Horizon research and innovation program (grant no. 101136091).

References

[1] M Becker, D Allaerts, and JW Van Wingerden. "FLORIDyn-A dynamic and flexible framework for real-time wind farm control". In: *Journal of Physics: Conference Series*. Vol. 2265. 3. IOP Publishing. 2022, p. 032103. DOI: 10.1088/1742-6596/2265/3/032103.

[2] M. Becker et al. "A dynamic open-source model to investigate wake dynamics in response to wind farm flow control strategies". In: *Wind Energy Science Discussions* (2024), pp. 1–32. DOI: 10.5194/wes-2024-150.

[3] M. Becker et al. "The revised FLORIDyn model: implementation of heterogeneous flow and the Gaussian wake". In: *Wind Energy Science* **7**.6 (2022), pp. 2163–2179. DOI: 10.5194/wes-7-2163-2022.

[4] Tony Burton et al. *Wind energy handbook*. John Wiley & Sons, 2011. Chap. 3, pp. 39–136. DOI: https://doi.org/10.1002/9781119992714.ch3.

[5] Chenlu Han and Ryozo Nagamune. "Platform position control of floating wind turbines using aerodynamic force". In: *Renewable Energy* **151** (2020), pp. 896–907. DOI: https://doi.org/10.1016/j.renene.2019.11.079.

[6] Chenlu Han and Ryozo Nagamune. "Position control of an offshore wind turbine with a semi-submersible floating platform using the aerodynamic force". In: *2016 IEEE Canadian Conference on Electrical and Computer Engineering (CCECE)*. 2016, pp. 1–4. DOI: 10.1109/CCECE.2016.7726687.

[7] Jeffrey R. Homer and Ryozo Nagamune. "Physics-Based 3-D Control-Oriented Modeling of Floating Wind Turbines". In: *IEEE Transactions on Control Systems Technology* **26**.1 (2018), pp. 14–26. DOI: 10.1109/TCST.2017.2654420.

[8] Ali C. Kheirabadi and Ryozo Nagamune. "Modeling and Power Optimization of Floating Offshore Wind Farms with Yaw and Induction-based Turbine Repositioning". In: *2019 American Control Conference (ACC)*. 2019, pp. 5458–5463. DOI: 10.23919/ACC.2019.8814600.

[9] Ali C. Kheirabadi and Ryozo Nagamune. "Real-time relocation of floating offshore wind turbine platforms for wind farm efficiency maximization: An assessment of feasibility and steady-state potential". In: *Ocean Engineering* **208** (2020), p. 107445. ISSN: 0029-8018. DOI: https://doi.org/10.1016/j.oceaneng.2020.107445.

[10] Ali C. Kheirabadi and Ryozo Nagamune. "Real-time Relocation of Floating Offshore Wind Turbines for Power Maximization Using Distributed Economic Model Predictive Control". In: *2021 American Control Conference (ACC)*. 2021, pp. 3077–3081. DOI: 10.23919/ACC50511.2021.9483056.

[11] Yue Niu et al. "Floating Offshore Wind Farm Control via Turbine Repositioning: Unlocking the Potential Unique to Floating Offshore Wind". In: *IEEE Control Systems* **44**.5 (2024), pp. 106–129. DOI: 10.1109/MCS.2024.3432342.

[12] Amy Robertson et al. *Definition of the semisubmersible floating system for phase II of OC4*. Tech. rep. National Renewable Energy Lab.(NREL), Golden, CO (United States), 2014.

[13] The European Commission. *An EU Strategy to harness the potential of offshore renewable energy for a climate neutral future*. COM/2020/741 final. The European Commission, 2020.